Analytical Methods

ROYAL SOCIETY OF CHEMISTRY

TECHNICAL NOTE

View Article Online
View Journal | View Issue

Cite this: *Anal. Methods*, 2025, **17**, 5519

Concentration dependence of Kubelka–Munk function and apparent absorbance button sample holder infrared spectra

Robert L. White *

Button sample holder infrared spectra in Kubelka–Munk function and apparent absorbance formats are evaluated. Trends in plots of vibration band area and peak intensity *versus* concentration are compared. Two test sample powders were comprised of different concentrations of caffeine dispersed in potassium chloride and copper thiosulfate mixed with kaolinite and potassium chloride in different ratios. When infrared spectra of caffeine and copper thiosulfate were measured by diffuse reflection, Kubelka–Munk calibration functions tended to be linear whereas apparent absorbance functions were curved. However, over narrow concentration ranges, both formats provided linear plots and exhibited similar sensitivities. For samples with the highest clay content, the kaolinite O–H stretching and inorganic oxide vibration band area *versus* concentration plots were linear over wider ranges than the Kubelka–Munk function plots.

Received 4th May 2025
Accepted 16th June 2025

DOI: 10.1039/d5ay00758e

rsc.li/methods

1. Introduction

Since its introduction in 2020,[1] the button sample holder has mainly been used to study temperature-dependent changes in solid-state materials by infrared spectroscopy.[2–6] The sample holder consists of a reflective stainless-steel disk to which a round piece of stainless-steel wire mesh is affixed.[1] Powdered samples are loaded into the wire mesh void spaces. Because both the wire mesh and sample redirect incident radiation over a wide range of angles, a diffuse reflection optical system is employed to collect the reflected light. Interactions between incident infrared radiation and particles contained in the sample holder are the same as those that occur in conventional diffuse reflection measurements.[7] However, when compared to traditional diffuse reflection infrared spectroscopy, the button sample holder method utilizes much thinner samples and the wire mesh introduces reflecting surfaces that are not present in the larger volumes of sample powder typically employed for conventional measurements. Thus, it might be expected that the Kubelka–Munk function,[7] which is commonly used to represent diffuse reflectance spectra, may not be applicable for button sample holder measurements.

The Kubelka–Munk function (eqn (1)) relates the sample absorption ($k_{\bar{\nu}}$) and scattering ($s_{\bar{\nu}}$) coefficients to the measured reflectance ($R_{\infty,\bar{\nu}}$).[8–10] This function is directly proportional to the absorptivity ($a_{\bar{\nu}}$) and the concentration (c) of the analyte at a particular wavenumber.

$$F(R_{\infty,\bar{\nu}}) = \frac{(1-R_{\infty,\bar{\nu}})^2}{2R_{\infty,\bar{\nu}}} = \frac{k_{\bar{\nu}}}{s_{\bar{\nu}}} = \frac{2.303\ a_{\bar{\nu}}c}{s_{\bar{\nu}}} \quad (1)$$

Among the assumptions made in deriving this equation is the "infinite" sample thickness approximation.[8] This requirement is satisfied when a scattering sample has sufficient thickness to prevent radiation from passing through it. Wavenumber-dependent infinite thickness thresholds depend on band absorptivity, the concentration of the sample, and the scattering coefficient.[11] In general, when radiation absorption increases, the infinite thickness threshold decreases. Radiation absorption is higher at wavenumbers where analyte absorptivity is larger and when sample concentration is greater.

Infrared radiation striking the surface of a powder can undergo specular reflection at the air/sample interface or penetrate the random distribution of particles, where scattering and absorption can occur. Unlike transmission measurements, radiation path lengths are not constant for diffuse reflection and diffuse transmittance. Instead, they depend on particle size, packing density, and sample thickness. In addition to these sample properties, the refractive indices, concentrations, and absorptivities of the analyte and diluent affect the relative intensities and widths of infrared spectrum bands. When a sample is diluted in a non-absorbing matrix, radiation can travel several millimeters before emerging.[11] In an absorbing matrix, average radiation travel distances are shorter because radiation that traverses long distances is completely absorbed and therefore does not contribute to the calculated mean.[12]

Apparent absorbance (eqn (2)) is an alternative format for representing diffuse reflectance infrared spectra.[13]

Department of Chemistry & Biochemistry, University of Oklahoma, 73019, USA. E-mail: rlwhite@ou.edu

$$\text{Apparent absorbance} = \log_{10}\left(\frac{1}{R_{\infty,\bar{\nu}}}\right) \quad (2)$$

This approach effectively applies Beer's law to diffuse reflection measurements. Even though the requirements for Beer's law are not met by the diffuse reflection process, the apparent absorbance format can be useful when samples are highly absorbing or when the Kubelka–Munk function is non-linear.[14–17]

Two benchmark studies have been conducted to evaluate the quantitative analysis capabilities of the button sample holder. Linear plots of Kubelka–Munk function band area *versus* concentration were obtained over a 1.25–10% (w/w) concentration range for mixtures of benzoic acid dispersed in KBr and for ammonium chloride after evaporating the methanol solvent from solutions containing between 1.25 and 20% solute.[18] The quantitative analysis capabilities and limitations of button sample holder infrared spectroscopy measurements are investigated in more detail here. The Kubelka–Munk function and apparent absorbance spectrum representations are compared for analytes mixed with non-absorbing and absorbing substances.

2. Experimental

Caffeine (CAS: 58-08-2), potassium chloride (CAS: 7447-40-7), and copper thiocyanate (CAS: 1111-67-7) were obtained from Sigma Aldrich (St Louis, MO). Powdered kaolinite (CAS: 1318-74-7) from Twigg County, Georgia was purchased from Ward's Natural Science (Rochester, NY).

The copper thiocyanate (CuSCN) and kaolinite powders consisted of very fine particles and were used as received. The caffeine and potassium chloride (KCl) powders were thoroughly ground by using a mortar and pestle to obtain particle sizes near 1 μm. A reference standard was prepared by mixing the ground caffeine and KCl powders to obtain a 19.3% (w/w) caffeine concentration. Additional standards were prepared by diluting the 19.3% standard with sufficient KCl to make mixtures containing: 0.5, 1.0, 2.6, 5.0, 7.7, 10.0, and 15.0% caffeine. A similar approach was employed to prepare standards containing CuSCN and kaolinite. A 20% (w/w) mixture of kaolinite and KCl was prepared. Varying amounts of CuSCN were then added to this kaolinite/KCl mixture to prepare samples with CuSCN concentrations (w/w) of 1.0, 2.5, 5.0, 7.5, 10.0, 12.5, 15.0, 20.0, 25.0, and 37.5%. The corresponding kaolinite concentrations (w/w) were: 19.8, 19.5, 19.0, 18.5, 18.0, 17.5, 17.0, 16.0, 15.0, and 12.5%.

A Mattson Instruments Inc. (Madison, WI) Nova Cygni 120 Fourier transform infrared (FTIR) spectrophotometer and a Harrick Scientific Inc. (Pleasantville, NY) praying mantis diffuse reflection accessory[19] were used for infrared spectroscopy measurements. The FTIR employed a water-cooled infrared radiation source and liquid nitrogen cooled MCT detector with a signal cutoff below 650 cm^{-1}. For the caffeine samples, spectra were obtained over the 4000–700 cm^{-1} range by signal averaging 64 scans at 8 cm^{-1} resolution for both sample and background single beam measurements. Infrared spectra for the CuSCN/kaolinite/KCl samples were measured by using the same wavenumber range and resolution, but by signal averaging 16 interferograms for sample and background single beam spectra. Although all measurements were made at 8 cm^{-1} resolution, interferogram zero filling prior to Fourier transformation yielded a 0.97 cm^{-1} spectrum digitization interval. This spectral resolution and digitization interval were sufficient to accurately represent small changes in the broad vibration bands and afforded greater spectral signal-to-noise ratio compared to higher resolution measurements.[20] The infrared spectrophotometer was purged with dry air to reduce artifacts caused by fluctuations in water vapor and carbon dioxide concentrations.

Fig. 1 shows a photograph of the button sample holder employed for the studies described here. The stainless-steel wire mesh was obtained from TWP Inc. (Berkeley, CA). The mesh was spot welded to the metal backing within a 6 mm diameter indentation in the disk. The wire screen had 100 square openings per inch (*i.e.* 100-mesh) formed by 114 μm diameter stainless-steel wires woven in a plain weave pattern. Each opening in the 100-mesh screen had dimensions of *ca.* 140 μm × 140 μm.

The depth of the indentation in the recessed 100-mesh button was 270 μm and the mesh thickness was 220 μm, so the distance between the top of the mesh and the upper surface of the stainless-steel button disk was about 50 μm. Thus, by filling the recessed 100-mesh button with sample to a level reaching the top surface of the disk, the powder thickness varied from 50 μm for particles directly above the mesh wires to 270 μm for particles occupying mesh void spaces. Less than 10 mg of KCl was required to completely fill the indentation containing the wire mesh. For comparison, the Harrick Scientific Inc. diffuse reflection accessory was supplied with a standard cup, which had a 14.0 mm inside diameter and a depth of 3.0 mm, and

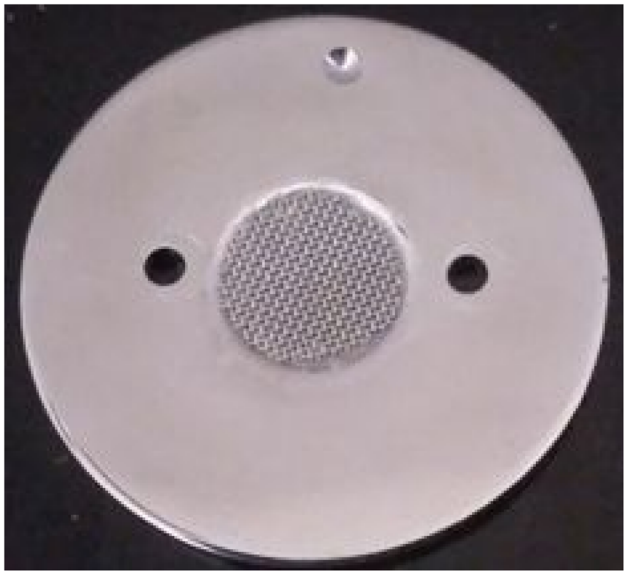

Fig. 1 Photograph of the button sample holder.

a microsampling cup, with a 3.5 mm inside diameter and 3.0 mm depth. About 500 mg of KCl was required to fill the standard cup and the microsampling cup capacity was about 30 mg.

3. Results

Fig. 2 shows mesh photographs comparing the empty button, after adding some caffeine/KCl powder, and after completely filling the sample holder so that the mesh wires were covered. Partially filling the button yielded non-uniform sample thicknesses and exposed the top surfaces of the highly reflecting mesh wires. Infrared spectrum measurement repeatability was poor when the button was partially filled because particle distributions throughout the mesh void spaces could not be adequately replicated. The most reproducible spectra were obtained when the sample holder was filled so that no wire surfaces were exposed. Consequently, all infrared spectra were measured after completely filling the sample holder. Complete filling was accomplished by pressing sample powders into the button indentation until all void spaces within the mesh were filled. Additional powder was then added to completely cover the wire mesh. A flat blade spatula was then used to level the powder with the top of the button metal disk and create a uniform smooth surface. The photograph on the right side of Fig. 2 shows typical results of using this sample loading procedure. Surface uniformity was important because imperfections can result in decreased diffuse scattering.[21,22]

3.1 Caffeine diluted in KCl

Infrared spectra were measured in triplicate for each of the eight caffeine/KCl samples. The 100-mesh button was emptied and refilled prior to successive spectrum measurements. Reflectance spectra were calculated by ratioing each single beam spectrum to the same pure KCl background single beam spectrum, which was measured prior to loading the first caffeine/KCl sample. The infrared spectra obtained for these samples are shown in Fig. 3 in apparent absorbance and Kubelka–Munk formats. Band maximum wavenumber locations are consistent with previously reported vibration band assignments for caffeine.[23] Intensities for all bands increased with increasing caffeine concentration in the spectra displayed in either format. However, relative band intensities were different, with the Kubelka–Munk format providing sharper bands and better discrimination between high and low absorptivity peaks.

Fig. 4a shows plots of the total integrated intensity of the spectra in Fig. 3 (*i.e.* 3400–700 cm^{-1}) as a function of caffeine content. The red plot was computed from apparent absorbance spectra and the blue plot was derived from the Kubelka–Munk spectra. The red line connects triplicate average area values calculated for each sample concentration and the blue line is the result of a linear regression computed from triplicate average Kubelka–Munk spectrum areas derived from samples containing less than 15% caffeine. Over the 0.5–10% range, a straight-line relationship was obtained between Kubelka–Munk integrated intensities and sample concentrations. In contrast, the apparent absorbance plot was curved over the entire concentration range. Fig. 4b shows the results obtained by integrating the C═O stretching vibration band intensities over the 1580–1520 cm^{-1} range. Although not the most intense in the spectrum, the C═O stretching vibration band intensity was among the highest. It was selected because it was more separated from neighboring vibration bands than the most intense bands. The trends in the Fig. 4b plots are similar to those obtained by integrating over 3400 – 700 cm^{-1} (Fig. 4a).

Fig. 5 shows plots of average infrared spectrum intensities at selected band maximum wavenumbers as a function of caffeine concentration. Plots derived from apparent absorbance spectra (Fig. 5a) are curved, with greater curvature exhibited by higher intensity bands. The Kubelka–Munk 1700 cm^{-1} band intensity plot is also curved (Fig. 5b), but not as much as the 1700 cm^{-1} apparent absorbance plot. The Kubelka–Munk 1550 cm^{-1} C═O stretching vibration band intensity plot is linear at low concentrations and curved at caffeine concentrations exceeding 10%. The 1025, 3110, and 700 cm^{-1} Kubelka–Munk band intensity plots exhibit linearity over the entire 0.5–19.3% concentration range.

Fig. 4 and 5 show that the Kubelka–Munk function provided better caffeine calibration curve linearity than apparent absorbance when samples were diluted in KCl. Also, plot linearity extended to higher concentrations when band intensities were lower.

Averett and Griffiths measured absorptivity values for some of the caffeine infrared spectrum vibration bands.[12] By using these values for the 1700 and 1025 cm^{-1} bands (*i.e.* 2460 and

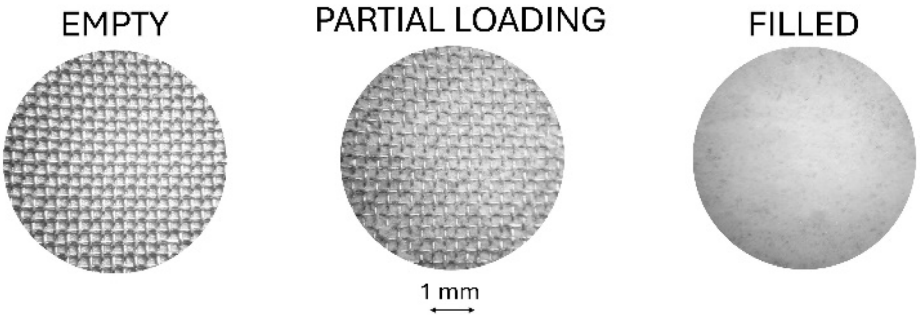

Fig. 2 Photographs of the empty (left), partially filled (center), and filled (right) button sample holder.

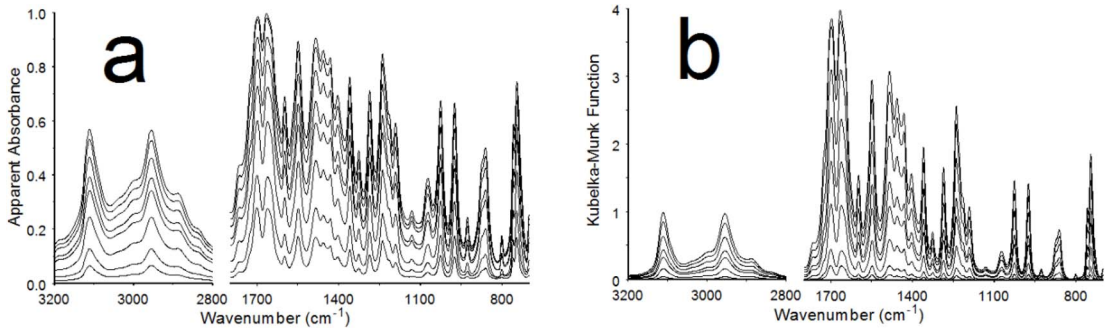

Fig. 3 Caffeine infrared spectra represented in (a) apparent absorbance and (b) Kubelka–Munk function formats.

290 cm^{-1} respectively) and the apparent absorbance intensities from Fig. 3a, the infrared transmission spectroscopy sample thickness required to produce the equivalent absorbances were derived from Beer's law for each caffeine/KCl mixture. Fig. 6 shows that the calculated radiation penetration distances (*i.e.* the equivalent transmission measurement path lengths) decreased exponentially with increasing caffeine concentration. The transmission spectroscopy equivalent path lengths calculated for the 1700 and 1025 cm^{-1} peaks were 0.23 and 0.70 mm for the 0.5% caffeine sample. These values are close to the 0.25 and 1.0 mm values estimated from the graphs provided by Averett and Griffiths.[12] Thus, although the button contained much less material than typically needed to fill a diffuse reflection sample cup, the caffeine infrared spectrum band intensities were similar. The distances plotted in Fig. 6 are estimates of the average radiation path lengths through the powder samples. Radiation travel distances were longer at 1025 cm^{-1} because the absorptivity was significantly less than at 1700 cm^{-1} (by a factor of ~8.5). At concentrations above 5%, average sample penetration distances at 1700 and 1025 cm^{-1} were less than the maximum sample thickness. For the 0.5% caffeine sample, the 230 μm equivalent path length at 1700 cm^{-1} was also less than the 270 μm maximum sample thickness in the button sample holder but the 700 μm 1025 cm^{-1} distance was more than twice the maximum thickness. Thus, 1025 cm^{-1} radiation could not have simply passed through the sample and reflected back from the button metal backing. Instead, it must have undergone significant lateral scattering before emerging from the sample.

3.2 Mixtures of CuSCN and kaolinite

To compare the apparent absorbance and Kubelka–Munk function spectrum representations for more complicated samples, mixtures containing different amounts of copper thiocyanate (CuSCN) and kaolinite were analyzed. Strong inorganic oxide absorption bands often exhibit the reststrahlen (residual rays) effect, in which reflectance near the band maximum is greater than expected.[24,25] After converting from reflectance to apparent absorbance or the Kubelka–Munk function, the intensities of bands exhibiting the reststrahlen effect are lower than expected based on molar absorptivities.[24] This effect, which is evident in kaolinite neat sample spectra, can be avoided by diluting the material in a non-absorbing matrix.[25] Thus, CuSCN and kaolinite mixtures were diluted in KCl to prevent reststrahlen effects in measured spectra. To avoid excessive absorption of infrared radiation, samples contained sufficient KCl powder to limit the kaolinite and CuSCN maximum concentrations to 20 and 37.5%, respectively. All single beam spectra were ratioed against the same previously acquired pure KCl background single beam spectrum. The most intense CuSCN infrared spectrum band at 2158 cm^{-1} corresponded to the C–N stretching vibration.[26] Intense kaolinite bands were associated with O–H stretching vibrations between

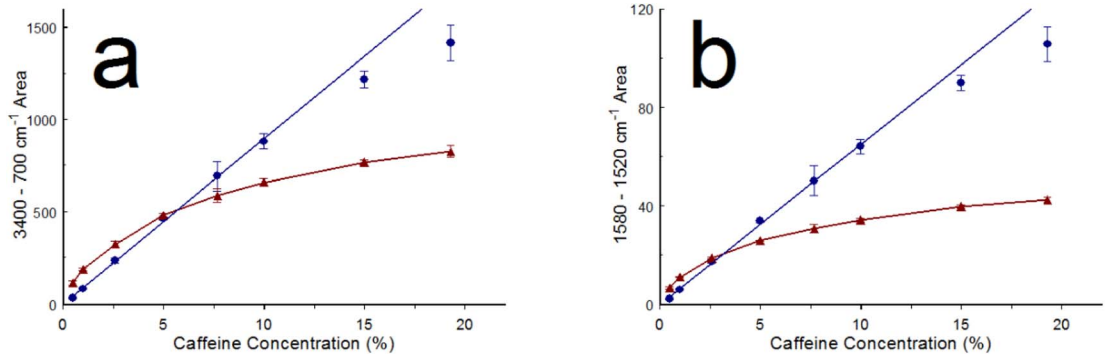

Fig. 4 Integrated band intensities as a function of caffeine concentration over the (a) 3400–700 cm^{-1} and (b) 1580–1520 cm^{-1} ranges derived from apparent absorbance (red) and Kubelka–Munk function (blue) spectra.

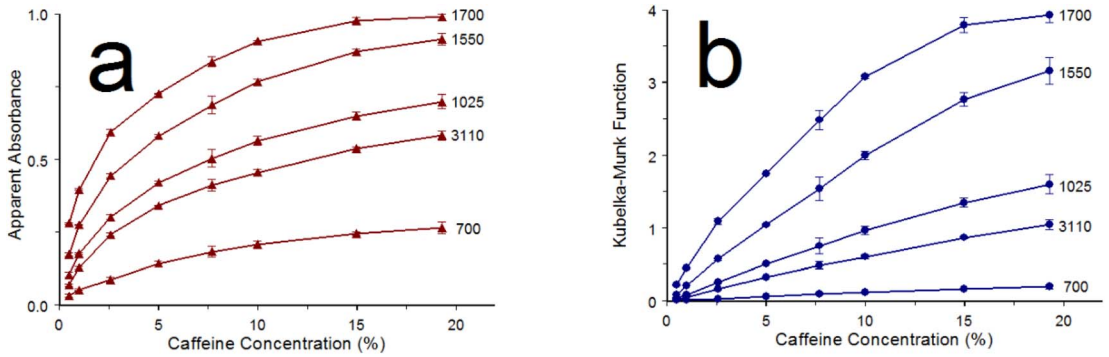

Fig. 5 Band intensity *versus* caffeine concentration plots derived from (a) apparent absorbance and (b) Kubelka–Munk function spectra.

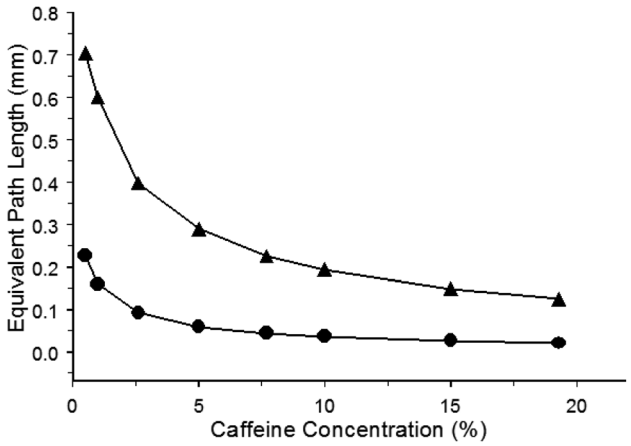

Fig. 6 Equivalent transmission spectrum radiation path length *versus* caffeine concentration plots derived from the 1700 cm^{-1} (circles) and 1025 cm^{-1} (triangles) apparent absorbance band intensities.

3750 and 3600 cm^{-1} and Si–O–Si stretching and Al–O–H bending vibrations of the inorganic oxide mineral between 1150 and 900 cm^{-1}.[3] Samples contained between 0 and 37.5% CuSCN and between 12.5 and 20% kaolinite. Sample mixtures were prepared so that when the CuSCN concentration increased, the kaolinite concentration decreased. Fig. 7 shows overlays of the apparent absorbance and Kubelka–Munk function infrared spectra. The blue arrow next to the C–N stretching vibration band at 2158 cm^{-1} indicates increasing intensity for the overlayed spectra. This trend is observed when viewing spectra derived from samples containing successively increasing CuSCN concentrations. In this instance, the decreasing kaolinite content results in decreasing band intensities, which is denoted by the two red arrows. Comparing the apparent absorbance and Kubelka–Munk spectra in Fig. 7 reveals the same trends that are observed in the caffeine infrared spectra (Fig. 3). The Kubelka–Munk spectra exhibit sharper peaks and provide better discrimination between high and low intensity bands.

Fig. 8a shows plots of the C–N stretching vibration integrated band intensity (2188–2118 cm^{-1}) *versus* CuSCN concentration derived from apparent absorbance (red) and Kubelka–Munk function (blue) spectra. The upper *x*-axis denotes kaolinite concentration, which decreases with increasing CuSCN concentration (lower *x*-axis). Like the caffeine plots in Fig. 4, the red line connects triplicate average band area values whereas the blue line is the result of a linear regression of the Kubelka–Munk spectrum average areas excluding those derived from

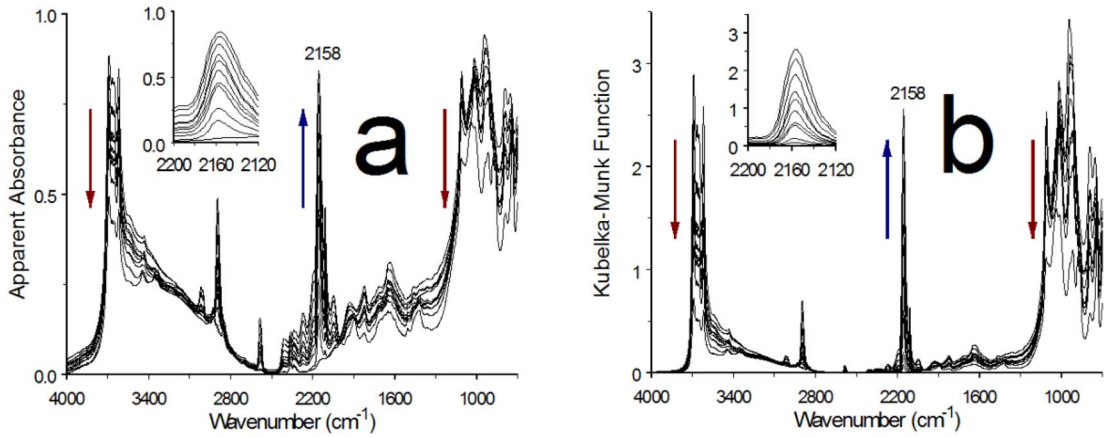

Fig. 7 CuSCN/kaolinite sample infrared spectra in (a) apparent absorbance and (b) Kubelka–Munk formats. Inset plots show scale expansions for the overlayed CuSCN 2158 cm^{-1} peaks.

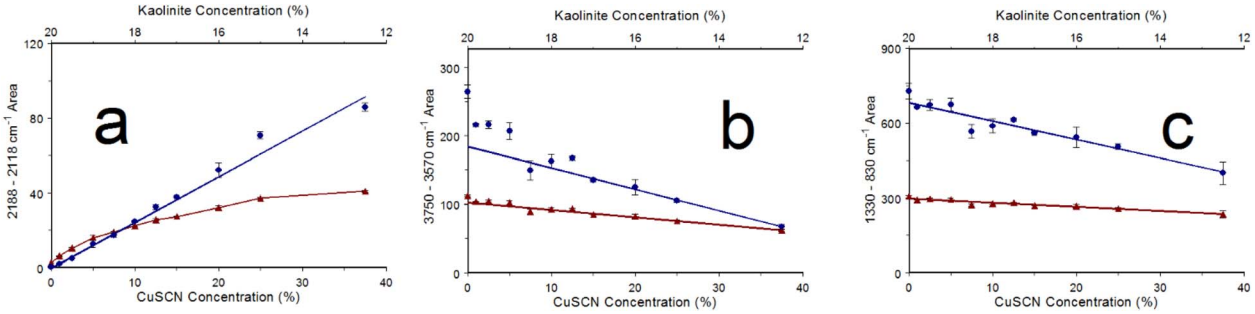

Fig. 8 Integrated band intensities between (a) 2188 and 2118 cm^{-1} for the CuSCN C–N stretching vibration band, (b) 3750 and 3570 cm^{-1} for the kaolinite O–H stretching vibration bands, and (c) 1330 and 830 cm^{-1} for the kaolinite inorganic oxide vibration bands plotted *versus* CuSCN concentration (bottom *x*-axis) and kaolinite concentration (top *x*-axis) derived from apparent absorbance (red) and Kubelka–Munk (blue) spectra. Kaolinite concentration decreases with increasing CuSCN concentration.

samples containing more than 10% CuSCN. The blue Kubelka–Munk plot is linear to about 15% CuSCN content whereas the apparent absorbance plot is curved over the entire concentration range.

Fig. 8b shows similar plots for the kaolinite O–H stretching vibration band areas. The red and blue lines were obtained by applying linear regressions to *x*–*y* pairs spanning the 12.5 to 17% kaolinite concentration range. The blue Kubelka–Munk plot exhibits a decreasing slope with substantially greater band area variability when samples contained more than 17% kaolinite. In contrast, the red apparent absorbance plot exhibits linearity up to 20% kaolinite content, but with a smaller slope. As shown in Fig. 8c, similar results were obtained by plotting the kaolinite inorganic oxide vibration band areas.

4. Discussion

For the caffeine samples, the Kubelka–Munk function was superior because it provided linear band area and intensity *versus* concentration plots. The Kubelka–Munk intensity *versus* concentration plots in Fig. 4b revealed a sensitivity *versus* linearity tradeoff. Linear calibration function regression slopes can be used to assess relative analytical sensitivities. Based on slope ratios, the sensitivity afforded by the 1025 cm^{-1} band intensity *versus* concentration plot was about 8 times greater than the 700 cm^{-1} plot sensitivity. However, the linear portion of the 700 cm^{-1} plot extended to higher caffeine concentrations. Thus, both linear concentration range and regression line slope should be considered when selecting Kubelka–Munk spectrum features that are best suited for quantitative assays.

Trends in Fig. 8a plots for CuSCN are similar to those observed for the caffeine samples. The Kubelka–Munk function provided a linear calibration plot up to a concentration of 15% whereas the apparent absorbance *versus* concentration plot was curved and flattened at high concentrations. In contrast, the kaolinite *versus* concentration apparent absorbance plots for the O–H stretching and mineral vibration bands were linear over the entire 12.5 to 20% concentration range whereas the Kubelka–Munk function plot linearity was limited to the 12.5–17% range. Note that most apparent absorbance *versus* concentration plots were also linear over the 10–20% ranges for caffeine (Fig. 4 and 5a) and CuSCN (Fig. 8a).

To compare the analytical sensitivities of the apparent absorbance and Kubelka–Munk functions over the 12.5 to 17% kaolinite concentration range, the ratio of the regression standard deviation to the calculated slope method[27] was employed:

$$\text{Sensitivity} = \frac{\sqrt{\sum_{i=1}^{n}\left(D_i - D_i^c\right)^2}}{\frac{n-2}{m}} \quad (3)$$

where D_i and D_i^c are the measured and regression calculated detector responses, n is the number of *x*–*y* pairs used for linear regression, and m is the regression line slope. This sensitivity metric is particularly useful when comparing calibration functions derived from different detection schemes because it incorporates information regarding the scatter of the data points about the regression line,[27] which depends on the detection response function. The calculated sensitivity represents the minimum concentration change that can be reliably detected over the regression interval. When applied to the regression lines in Fig. 8b, the apparent absorbance and Kubelka–Munk sensitivities were calculated to be 0.36 and 0.38% respectively over the 12.5–17% kaolinite concentration range. The regression plots in Fig. 8c yielded sensitivities of 0.30% for the apparent absorbance and 0.26% for the Kubelka–Munk function plots. Thus, although the Kubelka–Munk function provided greater regression line slopes than apparent absorbance, normalized sensitivities were comparable for both methods. Still, even though the sensitivities were similar, the apparent absorbance spectrum representation was superior because the linear range of the calibration function extended to higher kaolinite concentrations.

After penetrating the air/sample boundary, incident infrared radiation immediately begins to scatter in random directions. It has been estimated that diffuse scattering is achieved at depths of about 2 particle diameters from the sample surface.[11] At a sample depth of *ca.* 50 μm, diffusely scattered radiation could enter the button sample holder wire mesh void spaces. The volume of each square cylinder void space was: 140 μm × 140 μm × 220 μm = 4.3 × 10^6 μm^3 (4.3 × 10^{-6} cm^3). If all button

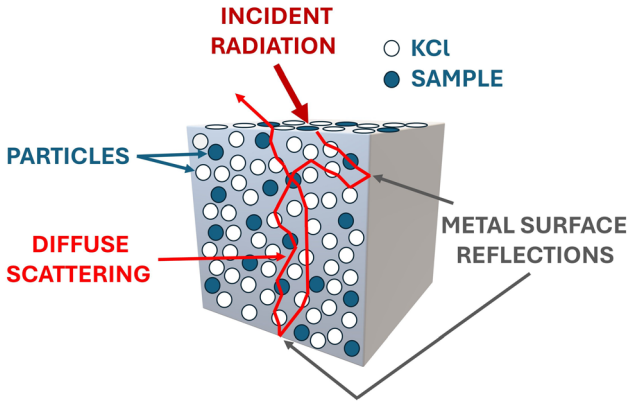

Fig. 9 Schematic of diffuse reflection through a square cylinder mesh void space.

sample holder void spaces were packed with sample material, roughly 490 square cylinders would be filled with about the same number of particles. However, because the infrared beam diameter at the focal point of the diffuse reflection optics was approximately 3 mm,[20] only about 110 of these square cylinders would be illuminated. The radiation entering these spaces would be restricted from lateral travel by reflections from the wires comprising the walls of each cylinder (Fig. 9). Thus, radiation could spread throughout the volume of each square cylinder but would be restricted from entering an adjacent cylinder. For conventional diffuse reflection measurements, the inside wall and floor of the sample cup are the only radiation obstructions, so lateral scattering is unrestricted until radiation reaches the cup wall. Consequently, for the same incident radiation beam size, the area from which diffusely scattered radiation emerges from the sample surface in a button sample holder should be smaller than that observed from a cup. As a result, the image formed at the detector focal point should be smaller when using a button sample holder. This is important because measurement signal-to-noise ratio suffers when the area of the radiation focused on the detector exceeds the detector area.[28] This phenomenon may explain why the caffeine infrared spectrum properties described here were similar to those previously obtained by using a sample cup[12] even though the amount of sample material employed was significantly less.

5. Conclusions

Button sample holders yield infrared spectra with characteristics like those obtained by using a diffuse reflection sample cup. In most instances, the Kubelka–Munk function is superior to apparent absorbance for representing button sample holder infrared spectra. Like conventional diffuse reflection, radiation can be absorbed when it penetrates particles and is scattered by reflections at particle surfaces and by refractions after passing through irregularly shaped particles. The volume of the stainless-steel wires that comprise the button mesh displaces particles, reducing the quantity of sample required to fill the sample holder. Additionally, reflections from these wires redirect radiation and contribute to light scattering. Thus, the mesh serves two purposes: it confines and isolates particles within small volumes; and it enhances radiation scattering. The properties of a mesh depend on the size and shape of the wires and the weave pattern. Because meshes are available in a wide variety of wire diameters and weave patterns, it is likely that certain mesh types are optimum for specific applications. Thus, additional studies to evaluate the characteristics of different types of meshes are warranted.

Data availability

Data is not archived but can be provided by the author.

Conflicts of interest

The author declares that there is no conflict of interest.

References

1 R. L. White, *Anal. Chim. Acta*, 2020, **1098**, 110–116.
2 J. Singh and R. L. White, *Spectrochim. Acta, Part A*, 2020, **231**, 118142.
3 H. F. Noneman, M. E. Hollingsworth, J. Singh and R. L. White, *Spectrochim. Acta, Part A*, 2021, **247**, 119113.
4 J. Singh and R. L. White, *Anal. Methods*, 2022, **14**, 1214–1220.
5 R. L. White, *Minerals*, 2023, **13**, 783.
6 H. F. Noneman and R. L. White, *Minerals*, 2024, **14**, 624.
7 J. P. Blitz, in *Modern Techniques in Applied Molecular Spectroscopy*, ed. F. M. Mirabella, Wiley, 1998, ch. 5, pp. 185–219.
8 P. Kubelka and F. Munk, *Z. Tech. Phys.*, 1931, **12**, 593–601.
9 P. Kubelka, *J. Opt. Soc. Am.*, 1948, **38**, 448–457.
10 A. A. Kokhanovsky, *J. Phys. D: Appl. Phys.*, 2007, **40**, 2210–2216.
11 D. J. J. Fraser and P. R. Griffiths, *Appl. Spectrosc.*, 1990, **44**, 193–199.
12 L. A. Averett and P. R. Griffiths, *Appl. Spectrosc.*, 2008, **62**, 377–382.
13 R. N. Clark and T. L. Roush, *J. Geophys. Res., B*, 1984, **89**, 6329–6340.
14 A. S. Yen, B. C. Murray and G. R. Rossman, *J. Geophys. Res.*, 1998, **103**, 11125–11133.
15 B. N. Olana, L. H. Adem, S. D. Lin, B. J. Hwang, Y. C. Hsieh, G. Brunklaus and M. Winter, *ACS Appl. Energy Mater.*, 2023, **6**, 4800–4809.
16 W. Zhang, T. Pu, Z. Wang, L. Shen and M. Zhu, *Ind. Eng. Chem. Res.*, 2022, **61**, 9678–9685.
17 R. T. So, N. E. Blair and A. L. Masterson, *Environ. Chem. Lett.*, 2020, **18**, 1725–1730.
18 J. Singh, PhD Dissertation, University of Oklahoma, 2021.
19 M. Milosevic and S. L. Berets, *Appl. Spectrosc. Rev.*, 2002, **37**, 347–364.
20 D. Maraoulaite and R. L. White, *Am. Lab.*, 2018, **50**, 14–17.
21 F. Boroumand, H. v. d. Bergh and J. E. Moser, *Anal. Chem.*, 1994, **66**, 2260–2266.
22 S. A. Yeboah, S. H. Wang and P. R. Griffiths, *Appl. Spectrosc.*, 1984, **38**, 259–264.

23 S. Gunasekaran, G. Sankari and S. Ponnusamy, *Spectrochim. Acta, Part A*, 2005, **61**, 117–127.
24 E. H. Korte and A. Roseler, *Anal. Bioanal. Chem.*, 2005, **382**, 1987–1992.
25 T. Iwaoka, S. H. Wang and P. R. Griffiths, *Spectrochim. Acta, Part A*, 1985, **41**, 37–41.
26 G. A. Bowmaker and J. V. Hanna, *Z. Naturforsch., B: J. Chem. Sci.*, 2009, **64**, 1478–1486.
27 L. C. Rodriguez, A. M. G. Campa[nbreve]Ta, C. J. Linares and M. R. Ceba, *Anal. Lett.*, 1993, **26**, 1243–1258.
28 T. Hirschfeld, *Appl. Spectrosc.*, 1985, **39**, 1085–1086.

